*Transactions*, SMiRT-25
Charlotte, NC, USA, August 4-9, 2019
Division III

# SIMULATION OF THE SURFACE FAULT OF THE 2014 NAGANO-KEN-HOKUBU EARTHQUAKE USING HIGH PERFORMANCE COMPUTING

**Masataka Sawada[1], Kazumoto Haba[2], Muneo Hori[3]**

[1] Research Engineer, Central Research Institute of Electric Power Industry, Abiko, Chiba, Japan (sawada@criepi.denken.or.jp)
[2] Manager, Taisei Corporation, Tokyo, Japan
[3] Director-General, Japan Agency for Marine-earth Science and Technology, Yokohama, Kanagawa, Japan

**ABSTRACT** Continuum mechanics-based numerical simulations are potential methods for evaluating surface fault displacements. We developed a parallel finite element method to evaluate these displacements. In this study, we applied a numerical method to simulate the 2014 Nagano-ken-hokubu Earthquake, in which surface faulting was observed. We modeled a 5 km × 5 km × 1 km domain around the northernmost region of the surface faults including secondary faults. We applied forced displacements on the bottom surface of the model based on the slip distribution on the primary fault and the elastic theory of dislocations. As the input slip increased, surface slips appeared along the primary fault and secondary faults. The calculated surface slips agreed well with the measured values. We also proposed a method to set slip distribution on primary faults for predictive simulations.

## INTRODUCTION

Since the occurrence of massive earthquakes in Taiwan and Turkey in 1999, there have been growing concerns regarding the potential damage to various infrastructure and buildings caused by surface fault ruptures. For on-site fault assessment at nuclear power plants, it is important to estimate fault displacements and their impact on facility safety functions.

Numerical simulations based on continuum mechanics are potential evaluation methods for surface fault displacements. However, there are major difficulties in simulating the fault rupture process. One is that it requires a large amount of numerical computations to simulate the fault rupture process of a target area of only a few hundreds of meters. Another difficulty is the stability loss in the initial boundary value problem to which the numerical analysis is applied. Stability implies that a solution does not change when a small disturbance is added to the problem, and stability loss leads to drastic changes in the solution because of small disturbances. We overcame these difficulties by applying high performance computing methods. We developed a finite element method (FEM) involving two functions: 1) a symplectic time integration explicit scheme to properly conserve the energy of the system and 2) rigorously formulated high-order joint elements. The FEM was enhanced with parallel computing capabilities (Sawada et al., 2017, 2018a).

We started applying this numerical method to the simulation of the 2014 Nagano-ken-hokubu Earthquake, in which surface faulting was observed (Sawada et al., 2018b). In this paper, we describe the results from the simulation of the earthquake using an updated analytical model and propose a method of setting input fault slip distribution for predictive simulation.

## METHOD

### *Estimation of fault displacement*

For the fault displacement simulations, we constructed a continuum model of the ground and faults (see Fig. 1). An input slip $\Delta$ was applied on the bottom of the primary fault (main fault) and the surface slip $\delta$ was obtained after calculating the spread and dispersion of the slip on the fault plane. For on-site fault assessment at nuclear power plants, surface slip on branch or secondary faults (sub-faults) must be estimated in addition to slip on the main fault.

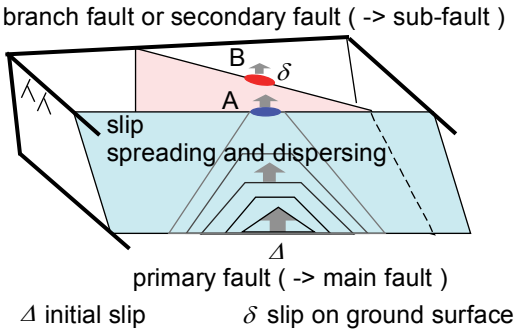


Figure 1. Spreading and dispersing of fault slip.

A fundamental difficulty in simulating the fault rupture process is the stability loss in the initial boundary value problem, which leads to significant changes in the solution because of small disturbances.

The treatment of uncertainties resulting from the limitations in the quality and quantity of the available relevant data for the underground structures, stress states, and source fault dynamics is important. Many simulations should be conducted under different conditions (capacity computing).

When considerable amounts of uncertainty exist, the surface fault displacement $\delta$ calculated by capacity computing is distributed over a wide range. In this case, $\delta$ is unpredictable in practice. It is important to evaluate the critical input slip $\Delta_c$, which is the minimum input slip that causes surface slip, before evaluating $\delta$.

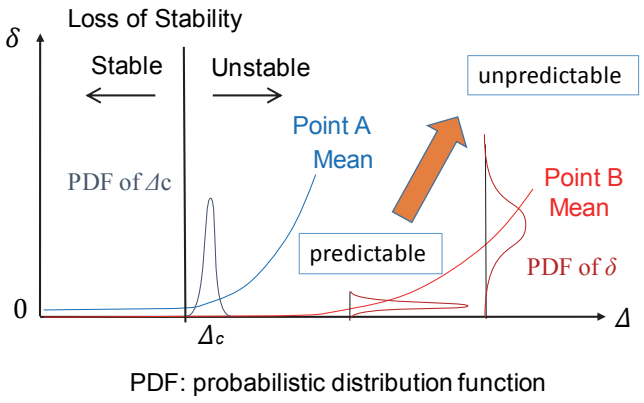


Figure 2. Prediction of surface fault displacement.

Quasi-static simulations allow a relationship between the input and surface slips to be determined. This is extremely important for the estimation of $\Delta_c$. Sawada et al. (2018) showed the calculated $\Delta_c$ and $\delta$ in the quasi-static simulations were near those calculated in the dynamic simulations with damping and proposed the use of quasi-static simulations for capacity computing. Quasi-static simulations were also applied in this study.

***FEM for the fault-displacement problem***

We implemented a rigorous joint element and symplectic time integration method with a Hamiltonian formulation in the open-source FEM program FrontISTR (FrontISTR Commons, 2018) to develop a numerical tool for simulating fault displacements.

In joint elements that are widely used in the field of rock mechanics, nodal forces are directly calculated from relative nodal displacements on a discontinuity (e.g., Goodman et al., 1968). Using this method, the element stiffness matrices are easily calculated. However, they differ from the standard method for constructing finite elements. Joint elements for fault-displacement simulations should be obtained to ensure proper convergence for the chosen element sizes and applicability to curved faults. We developed a rigorous joint element in which the element stiffness matrices were derived from the Lagrangian on the discontinuous surface using an isoparametric formulation (Sawada et al., 2017).

We implemented the joint elements with a nonlinear spring-type constitutive equation to represent the fault movement. The following is the constitutive equation for shear movement of the joint element:

$$\tau = \kappa u$$

where $\tau$ is the shear stress and $u$ is the slip on the fault plane. The spring coefficient per unit area (shear stiffness) $\kappa$ is described by the following function of the slip $u$:

$$\kappa(u) = \begin{cases} \kappa_0 - \dfrac{\kappa_0 - \kappa_d}{u_{cr}} u & (u \le u_{cr}), \\ \kappa_d & (u > u_{cr}), \end{cases}$$

where $\kappa_0$ is the initial shear stiffness, $\kappa_d$ is the final shear stiffness, and $u_{cr}$ is the critical slip (see Fig. 3). Notably, we did not use any sliders or dashpots in the model for $\kappa$.

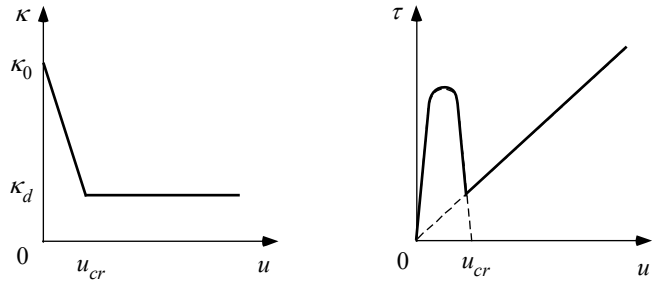


Figure 3. Frictional characteristics and slip-shear stress relation.

We considered the effect of the normal stress on the shear stiffness of the faults and defined the following equation:

$$\kappa_0 = a\sigma_n + b$$

where $a$ and $b$ are the constants and $\sigma_n$ is the normal stress on the fault plane.

## MODEL

### *Target earthquake*

We applied the numerical method to the November 22, 2014, Nagano-ken-hokubu Earthquake of Mj = 6.7 (Mw = 6.2). A 9-km-long surface rupture was observed on the previously mapped Kamishiro fault. Figure 4 shows the mapped location of the rupture in the northernmost section. Sub-faults were also observed, including Sub-E1, Sub-E2, Sub-N, and Sub-S as shown in Fig. 4. Figure 5 shows the net slip along the surface rupture estimated using airborne Light Detection and Ranging (LiDAR) data obtained at two different times (Aoyagi, 2016). The maximum net slip values on the main fault and sub-faults were approximately 1.5 and 0.6 m, respectively.

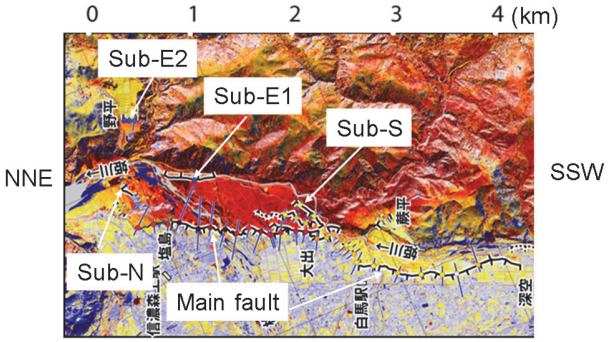


Figure 4. Distribution of surface ruptures in the northernmost section, modified after Aoyagi (2016).

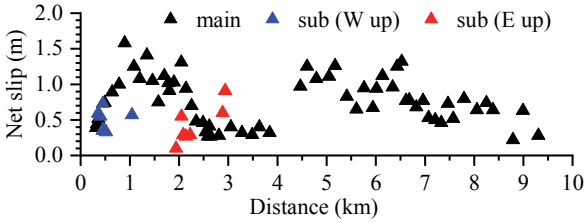


Figure 5. Surface fault dislocation from Aoyagi (2016). The horizontal axis corresponds to the distance from the northern end of the surface rupture, the scale of which is equivalent to that of Fig. 4.

### *Model*

We determined the mechanical properties of the ground and strike angle of the main fault based on the Japan Seismic Hazard Information Station (J-SHIS) database, developed by the National Research Institute for Earth Science and Disaster Resilience (NIED) and covering all of Japan.

Figure 6 shows a finite element mesh used for the simulation. The target was a 5 km × 5 km region around the northern end of the surface rupture. The depth of the domain was approximately 1 km.

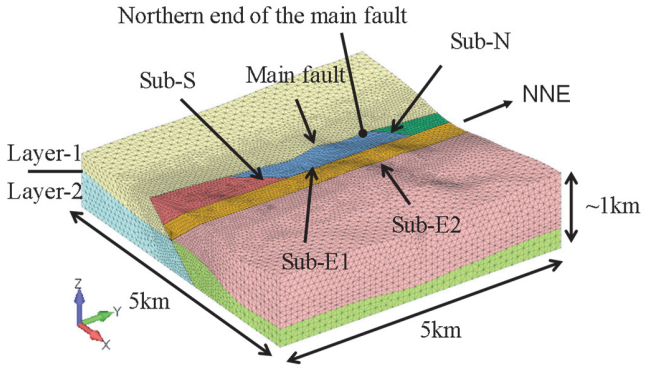


Figure 6. Finite element mesh

We included one main fault and four sub-faults. The Sub-E2 fault is newly included in the model this time. The dip angle of the main fault was 40°. Sub-E1 and Sub-E2 had the same strike angle as the main fault, and a dip angle of 40° in the opposite direction. Sub-N and Sub-S had strike angles of 45° from the main fault and 45° from the northside and southside of the dip angles, respectively. The ground was discretized by second-order tetrahedral elements and the fault planes were discretized by second-order triangle joint elements. The size of the elements on the fault planes was approximately 50 m and the total number of degrees of freedom was approximately 2.58 million.

The Geospatial Information Authority of Japan (GSI) derived a slip distribution on the main fault from the crustal movements estimated by differential interferometric synthetic aperture radar (DInSAR) as shown in Fig. 7 a). GSI's main fault had dip angles of 40° and 60° in the shallow and deep parts, respectively. We re-evaluated the slip distribution of the shallow part of the main fault based on Aoyagi (2016). We used dislocation theory (Okada, 1985) with the slip distribution as the input and determined the forced displacements at the bottom of the model. The maximum slip on the bottom of the fault was 3.0 m, which was twice the estimated slip. The other outer boundaries of the model were traction free. We termed this simulation "reproductive simulation."

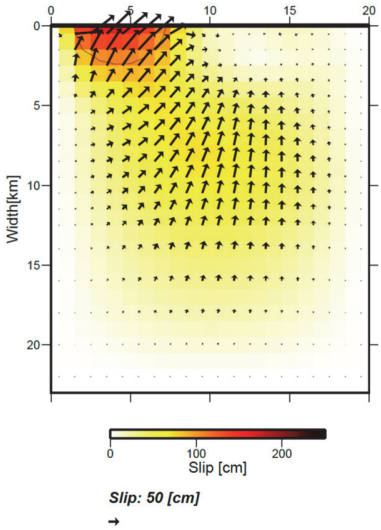


a) GSI (2015)

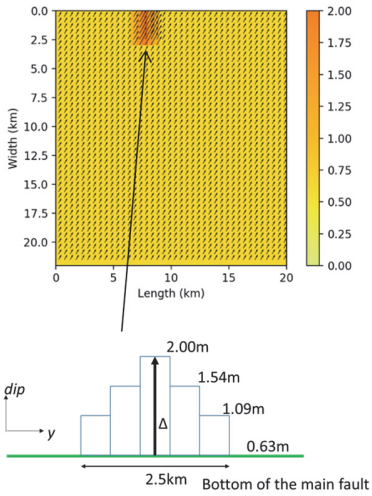


b) Setting for predictive simulation

Figure 7. Slip distribution on the main fault.

We must assume the slip distribution on the main fault in predictive simulations. We set the slip distribution in reference to the strong motion prediction method termed "recipe" (the Headquarters for Earthquake Research Promotion, 2016), which has the following steps: (1) set the geometry (length, width, depth. and dip angle) of the main fault, (2) calculate the seismic moment, (3) calculate the average slip from the seismic moment and shear modules of the crust, and (4) set the number and location of the asperities and calculating the slip on them and the other background. In predictive simulation, we used the same geometry of the main fault through GSI (2015) and obtained 0.63 m of average slip in step (3). When we set only this average slip on the main fault, surface slip did not appear on the sub-faults. However, the slip along the surface fault was not generally uniform. Therefore, we set a large slip part on the main fault as shown in Fig. 7 b). We used the empirically obtained equation of $D = 10^{-4}L$ (where $D$ is the slip and $L$ is the surface rupture length) proposed in Matsuda et al. (1981) to set the maximum surface slip. Here, we substituted 20 km of fault length to $L$ and obtained a $D$ = 2.0 m. In the simulation, the maximum slip on the bottom of the fault was 4.0 m, which was twice that of $D$. We termed this simulation "predictive simulation."

The J-SHIS database includes elevational data regarding the ground surface and boundaries of the elastic wave velocity and density. Based on this information, we considered the shape of the land and the two layers of the ground. The Young's modulus and Poisson's ratio of each layer were determined from the elastic wave velocity and density. We assumed that the first peak of the slip-shear stress relation shown in Fig. 3 was identical to the shear strength. The initial shear stiffness $\kappa_0$ and coefficients were determined such that the shear strength satisfied Coulomb's law of friction with a cohesion of 0.025 MPa and a 25° friction angle. The ratio between the initial and final shear stiffnesses, $\kappa_d/\kappa_0$, was assumed to be 0.01 and the critical slip $u_{cr}$ 0.1 m.

## RESULT

### *Reproductive simulation*

Figure 8 shows the displacement norm contour and deformation of the analytical domain. Figure 7 a) and b) show the results at $\Delta$ = 1.5 and 3.0 m, respectively. The deformation is shown with 300-times amplification. Large deformation occurred at the center of the model where the input slip was large. There was a displacement gap along the main, the Sub-E1 and Sub-E2 faults, showing surface slip.

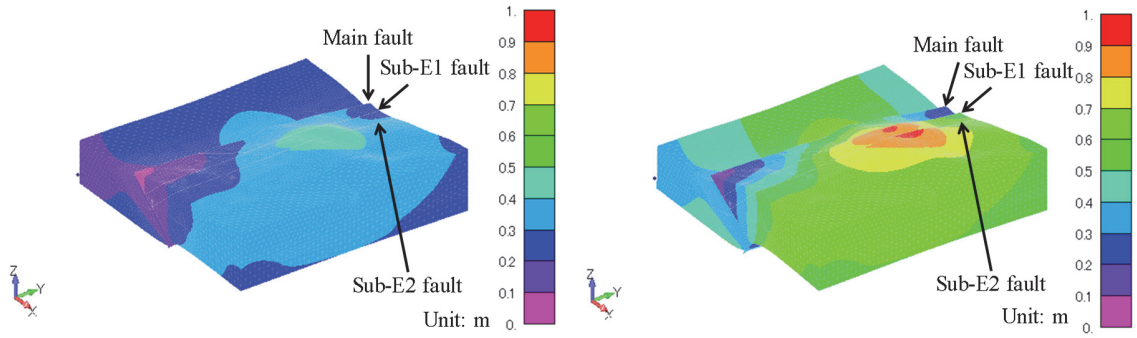


a) $\Delta$ = 1.5 m b) $\Delta$ = 3.0 m

Figure 8. Contours of displacement norm and deformation.

Figures 9 shows contour plots of the slip at $\Delta$ = 3.0 m on the main fault and sub-faults. This figure shows views from the +$x$ (east) side. There was a surface slip of greater than 1.0 m on the main fault and a

surface slip in the north sections of the Sub-E1 and Sub-E2 faults. In the simulation, the maximum surface slip was approximately 0.5 m on Sub-E1; this value was similar to the measured value shown in Fig. 5. The calculated surface slip was small on Sub-E2, Sub-S, and Sub-N. Overall, the simulated surface slip distribution at $\Delta$ = 3.0 m agreed well with the measured distribution.

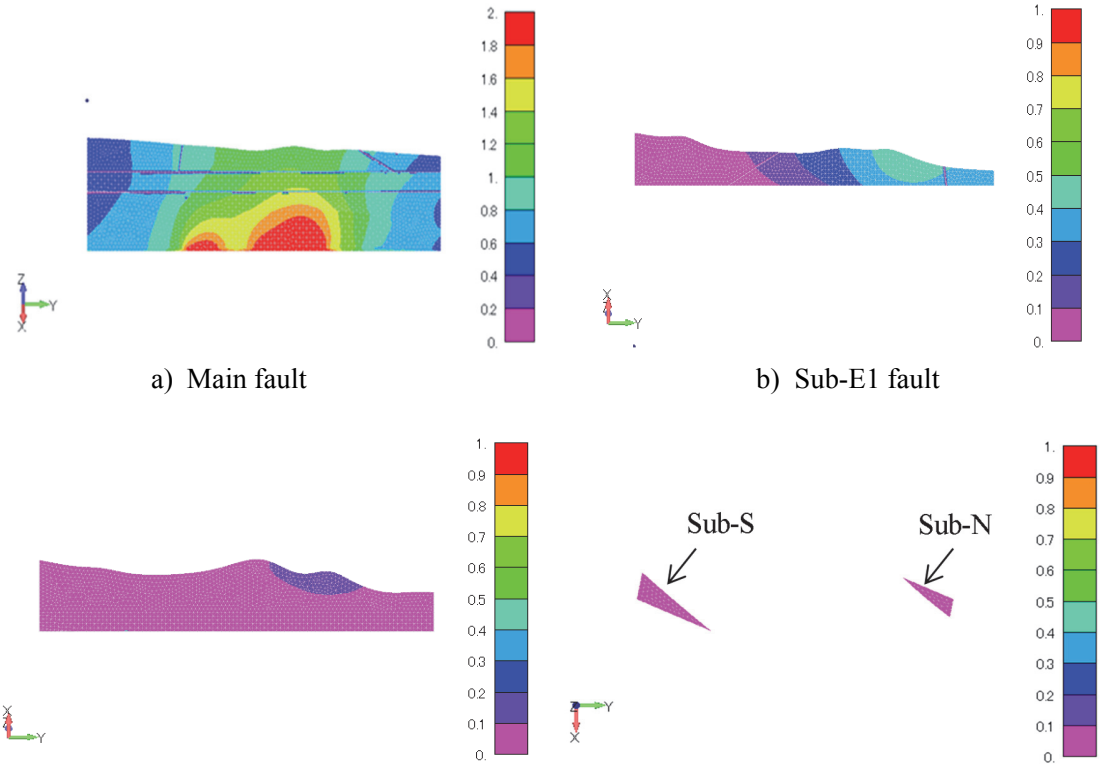


a) Main fault b) Sub-E1 fault

c) Sub-E2 fault d) Sub-S and Sub-N faults

Figure 9. Contours of slip on the main fault and sub-faults ($\Delta$ = 3.0 m).

Figure 10 shows the evaluation points for surface slip. In the legend, "main" and "sub" are abbreviations for the main and sub-faults, respectively, and "Y2000" is an abbreviation for the y-coordinate of 2000 m.

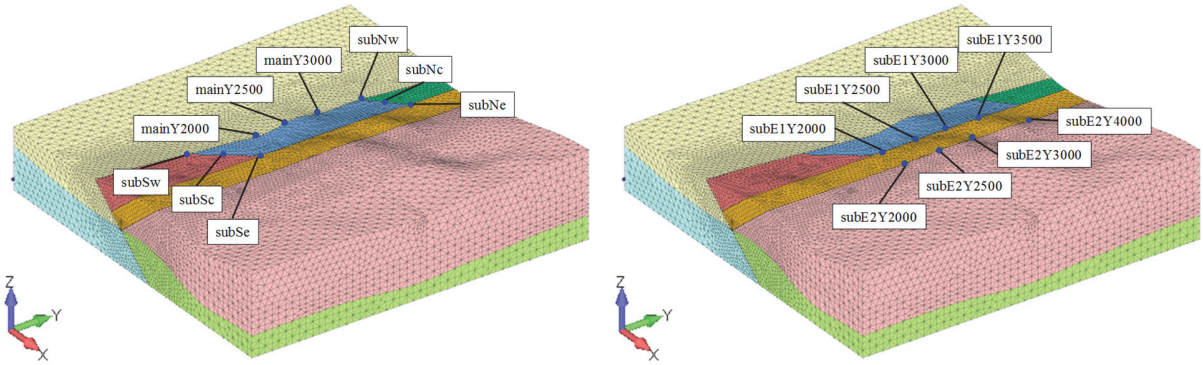


a) Main, Sub-S and Sub-N faults b) Sub-E1 and Sub-E2 faults

Figure 10. Evaluation points.

Figure 11 shows the variation in the surface net slip $\delta$ as the input slip $\Delta$ increases. There was a steep increase in the surface slip at $\Delta$ = 0.69 m on the main fault (mainY2500). A steep increase in the surface slip on the Sub-E1 fault (subE1Y3500) began at $\Delta$ = 2.58 m. Therefore, the critical slip $\Delta_c$ was 0.69 m on the main fault and 2.58 m on the Sub-E1 fault. On the Sub-E2 fault (subE2Y4000), there was not a steep increase, but the slip exceeded 0.1 m at $\Delta$ = 2.94 m.

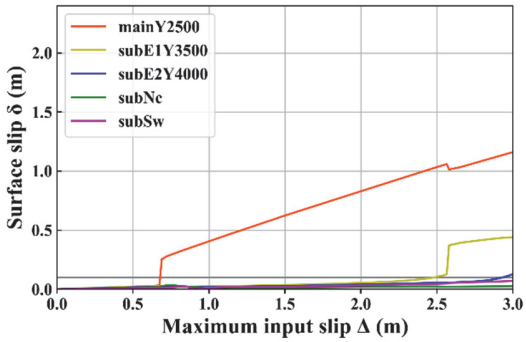


Figure 11. Surface slip-input slip relation.

Figure 12 shows the dip and strike-slip components of the surface slip at representative evaluation points of the main fault and sub-E1 fault. Positive strike slip means left-lateral slip and positive dip slip means normal fault sense. The dip slips on both the main and sub-E1 faults were negative. The two behaved as reverse faults. The Sub-E1 fault moved as though it was a back-thrust of the main fault. This movement agreed qualitatively with the observations. However, the dip component of the slip on the Sub-E1 fault was less than the measured value.

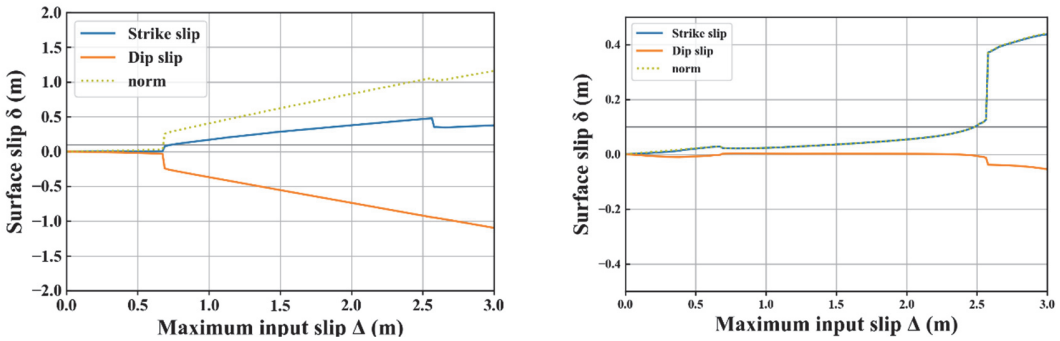


a) Main fault (mainY2500) b) Sub-E1 fault (subE1Y3500)

Figure 12. Strike and dip component of the surface slip.

***Predictive simulation***

Figure 13 shows the variation in the surface net slip $\delta$ as the input slip $\Delta$ increases in the predictive simulation. There was a steep increase in the surface slip at $\Delta$ = 0.64 m on the main fault (mainY2500) and at $\Delta$ = 2.88 m on the Sub-E1 fault (subE1Y3500). On the Sub-E2 fault (subE2Y4000), there was also a steep increase at $\Delta$ = 3.70 m. These $\Delta_c$ values agree well with those in the reproductive simulation.

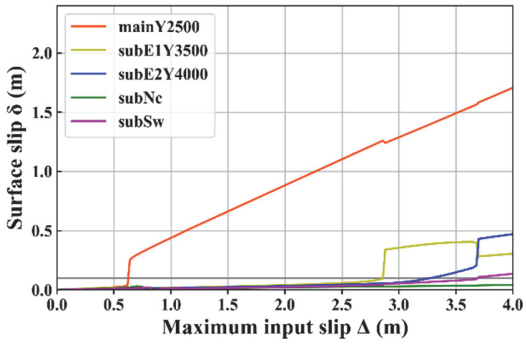


Figure 13. Surface slip-input slip relation in the predictive simulation.

***Discussion***

We constructed a 5 km × 5 km × 1 km analytical model and derived the boundary condition from the elastic theory of dislocation using slip distribution on the main fault obtained from inverse analysis of DInSAR and multi LiDAR-DEM data (reproductive simulation) or using the strong motion prediction method and assuming a large slip part (predictive simulation).

When we provided twice the inversely analyzed slip on the main fault to the bottom of the analytical domain, we obtained a steep increase in surface slip on the main fault and sub-faults. The final surface net slips agreed well with the measured values. The dip component of the slip on the Sub-E1 fault was qualitatively identical to the back-thrust-like movement observed at the site. Because the simulation reproduced the main features of the observed surface rupture, the proposed numerical method is applicable to surface fault displacement estimation.

However, some phenomena were not reproduced in the simulation. For example, surface slip did not appear on the Sub-N or Sub-S faults. One possible reason is that slip in the section in which $y > 3855.77$ m on the main fault was not restricted. It may be necessary to consider the spatial distribution of the fault friction properties to reproduce the surface slip on the Sub-N and Sub-S faults.

In the predictive simulation, we obtained similar results to those of the reproductive simulation. We consider that the slip distribution on the main fault determined from the proposed method is for a case in which surface slip on the sub-faults is likely to occur.

**CONCLUSION**

We developed a parallel FEM program to estimate surface fault displacement. In this study, we applied a numerical method to a simulation of the 2014 Nagano-ken-hokubu Earthquake in which surface faulting was observed. We modeled a 5 km × 5 km × 1 km domain around the northernmost region of the surface faults, including secondary faults. We applied the forced displacements on the bottom surface of the model based on the slip distribution on the primary fault and the elastic theory of dislocation. As the input slip increased, surface slip appeared on both the primary fault and a secondary fault. Calculated surface slips agreed well with those measured. Because the simulation reproduced the main features of the observed surface rupture, the proposed numerical method is applicable to surface fault displacement estimation. We also proposed a method to set the slip distribution on main faults as conditions under which surface slip on sub-faults is likely to occur for predictive simulation.

## ACKNOWLEDGEMENT

This study was supported by commissioned projects from the Agency for Natural Resources and Energy, Ministry of Economy, Trade and Industry, Japan.

## REFERENCES

Aoyagi, Y. 2016. Fault displacement distribution of the 2014 Nagano-ken-hokubu earthquake based on a differential analysis of multi LiDAR-DEM data. *Abstracts, Japan Geoscience Union Meeting*, SSS31-18. (in Japanese)

FrontISTR Commons. 2018. https://www.forntistr.org/, retrieved December 14, 2018. (in Japanese)

Geospatial Information Authority of Japan. 2015. https://www. jisihn.go.jp/main/chousa/14dec_nagano/p.29.htm, retrieved June 5, 2018. (in Japanese)

Goodman, R. E., Taylor, R. L. and Brekke, T. L. 1968. A model for the mechanics of jointed rocks. *J. ASCE* 94(SM3): 637–659.

Matsuda, T., Yamazaki, H., Nakata, T. and Imaizumi, T. 1981. The surface faults associated with the Rikuu Earthquake of 1896. *Bull. Earthqu. Res. Inst.*, *U. Tokyo* 55(3), 795–855. (in Japanese)

National Research Institute for Earth Science and Disaster Resilience. Japan Seismic Hazard Information Station. http://www.j-shis.bosai.go.jp/en/, retrieved June 5, 2018.

Okada, Y. 1985. Surface deformation due to shear and tensile faults in a half-space. *Bull. Seism. Soc. Am.* 75(4): 1135–1154.

Sawada, M., Haba, K. and Hori, M. 2017. High performance computing for fault displacement simulation. *J. JSCE* 73(2): I_699–I_710. (in Japanese)

Sawada, M., Haba, K. and Hori, M. 2018a. Estimation of surface fault displacement by high performance computing. *J. Earthqu. Tsun*12(4): 1841003 (22 pages)

Sawada, M., Haba, K. and Hori, M. 2018b. Evaluation of surface fault displacement in a real earthquake with surface faulting by high performance computing, *J. JSCE* 74(2): I_627–I_638. (in Japanese)

The Headquarters for Earthquake Research Promotion. 2016. Strong ground motion prediction method for earthquakes with specified source faults (“Recipe”).